Journal of Nuclear Materials 527 (2019) 151799

Contents lists available at ScienceDirect

Journal of Nuclear Materials

journal homepage: www.elsevier.com/locate/jnucmat

Effects of neutron irradiation on the brittle to ductile transition in single crystal tungsten

R.G. Abernethy [a, *], J.S.K.-L. Gibson [a], A. Giannattasio [a], J.D. Murphy [a, b], O. Wouters [c], S. Bradnam [d], L.W. Packer [d], M.R. Gilbert [d], M. Klimenkov [e], M. Rieth [e], H.-C. Schneider [e], C.D. Hardie [d], S.G. Roberts [a, d], D.E.J. Armstrong [a]

[a] Department of Materials, University of Oxford, Oxford, OX1 3PH, UK
[b] School of Engineering, University of Warwick, Coventry, CV4 7AL, UK
[c] Nuclear Research and Consultancy Group, Petten, the Netherlands
[d] CCFE, Culham Science Centre, Abingdon, OX14 3DB, UK
[e] Karlsruhe Institute of Technology, Karlsruhe, Germany

GRAPHICAL ABSTRACT

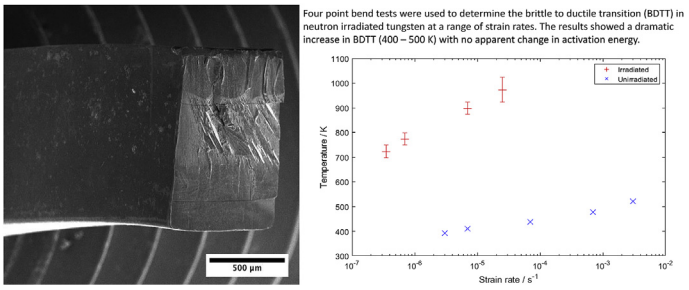

ARTICLE INFO

Article history:
Received 29 May 2019
Received in revised form
6 August 2019
Accepted 12 September 2019
Available online 12 September 2019

ABSTRACT

Only limited data exist on the effect of neutron irradiation on the brittle to ductile transition (BDT) in tungsten. This work investigates the increase in brittle to ductile transition temperature (BDTT) following neutron irradiation to 1.67 displacements per atom, using four-point bend tests over a range of temperatures (623–1173 K) and strain rates (3.5×10^{-7} - 2.5×10^{-5} s^{-1}). The BDTT was found to increase by 500 K after irradiation. The activation energy for the BDT was determined using Arrhenius analysis of the four-point bend tests. Nanoindentation strain-rate jump tests were used to characterise the activation volume for dislocation motion. These were quantified as 1.05 eV and 4.6 b^3 respectively, very close to values found for unirradiated tungsten. This suggests that kink-pair formation is the controlling mechanism for the BDT before and after irradiation. This work also carries out a unique verification of inventory-code-modelling (via FISPACT-II) of transmutation of tungsten to rhenium and osmium under neutron irradiation using two independent techniques (X-ray and gamma-ray spectroscopy). These results show that modelling can correctly predict this transmutation, provided that an accurate neutron spectrum is used. This is a critical result given the widespread use of inventory codes such as FISPACT-II, and the associated nuclear data libraries, for modelling transmutation of tungsten.

* Corresponding author.
E-mail address: robert.abernethy@ukaea.uk (R.G. Abernethy).

https://doi.org/10.1016/j.jnucmat.2019.151799

1. Introduction

Tungsten is the leading candidate as the plasma-facing material for first-wall and divertor applications in future nuclear fusion power plants, due to its high melting point (3695 K), low sputtering rates and good thermal conductivity [1]. However, there are concerns over its mechanical properties, in particular its low formability and high brittle to ductile transition temperature (BDTT) [2]. Work is ongoing for developing manufacturing routes for tungsten components such as cold-working [3] and tungsten composites [4] to improve ductility. These approaches have shown increasing promise in recent years [5,6].

There have been several studies of the fracture properties of tungsten [7,8] including its brittle to ductile transition (BDT), however there has been comparatively little work on the impact on neutron irradiation on the BDT. The BDT will be critical for determining the minimum operating temperature and lifetime of tungsten within a fusion power plant [9], where tungsten components may be exposed to >20 dpa during operation [10] at temperatures above 1073 K [9]. Even during the planned 14 years of ITER campaigns, tungsten components will be exposed to up to 0.5 displacements per atom (dpa) of irradiation damage [11]; the impact of this on the ductility of tungsten is not yet known. Any decrease in ductility as a result of irradiation may influence both operation of the device and end-of-life handling.

1.1. Brittle to ductile transition in unirradiated single crystal tungsten

The BDT in tungsten is controlled by the capability of dislocation motion to shield the crack tip. Below the BDTT, dislocation motion is limited and as a result the local stress can exceed the cohesive stress resulting in brittle fracture [12]. Above the BDTT, semi-brittle or ductile behaviour is observed with plastic deformation occurring before fracture.

Dislocation motion near a crack tip can be limited either by dislocation nucleation or dislocation mobility. Gumbsch et al. [13,14] showed that the BDT in single crystal tungsten was controlled by dislocation mobility around crack tips, rather than dislocation nucleation at crack tips. In this work the BDTT was measured as 370–470 K and the activation energy for the $\{110\}1\bar{1}0$ crack system was found to be 0.2 eV. This low activation energy was a consequence of the specific crystal orientation used during these experiments, favouring control of the BDT by the rapid motion of pure edge dislocations. The same controlling mechanism has been observed in ultra-fine grain tungsten [15].

Giannattasio and Roberts [16] investigated the $\{100\}001$ crack system and determined a BDTT range of 390–500 K (strain rate dependent) and an activation of 1.0 eV. In this work the same BDTT range and activation energy was found for pure polycrystalline tungsten, showing that this crack system is more representative of bulk tungsten.

Dislocation-dynamics modelling by Tarleton et al. [17] indicated that in the general case the BDT in tungsten is controlled by kink-pair mediated glide of 1/2<111> screw dislocations. This modelling showed that the activation energy for the BDT observed by Giannattasio and Roberts (1.0 eV) is the result of the kink-pair nucleation energy of 1.75 eV being reduced by the internal resolved shear stresses in the crack-tip dislocation arrays (326 MPa with an inferred activation volume of $20\,b^3$, where b is the magnitude of the Burgers vector).

An alternative interpretation has been provided by recent analysis by Swinburne and Dudarev [18] that predicted a single-kink formation energy is the characteristic activation energy for dislocation motion in microstructures with an obstacle spacing above a well-defined threshold value that is a function of temperature and stress. This threshold distance was shown to range from 10^{-2}–10^{1} μm for bcc iron (which shows similar BDT behaviour to that of tungsten) at realistic stresses and temperatures.

The material investigated by Giannattasio and Roberts was well-annealed single crystal. This suggests that the obstacle spacing should be above the threshold distance and so, according to Swinburne and Dudarev, a single kink energy close to 1 eV should be observed. This analysis agrees with the activation energy measured experimentally by Giannattasio and Roberts [16], if the energy contribution from stress acting on the dislocation is considered negligible. The relevance of this interpretation to this work is discussed further in section 1.4.

1.2. Effect of radiation damage on tungsten

One of the critical outstanding challenges for fusion materials is understanding the effects of neutron radiation on tungsten [5,19]. Within a fusion environment tungsten will be exposed to a high flux (up to $7 \times 10^{18}\,m^{-2}s^{-1}$) of high energy neutrons (up to 14 MeV) in addition to extreme heat fluxes (with peak loads of 10–20 MW $m^{-2}s^{-1}$ [20]) and implantation of hydrogen and helium ash ejected from the plasma. Interaction of the neutrons with tungsten nuclei causes transmutation of tungsten (predominantly to rhenium, osmium and tantalum [21]) and the kinetic energy of the neutrons causes collision cascades, resulting in the formation of excess vacancies and interstitials [22]. This excess of point defects results in the formation of dislocation loops and voids [23], and facilitates radiation enhanced segregation resulting in W-Re-Os precipitate formation [24,25]. This damage has been shown to result in significant hardening [26].

Due to the formation of W-Re-Os precipitates, accurate calculation of irradiation-induced transmutation is critical for understanding changes in properties under neutron irradiation [27]. The transmutation level is commonly calculated using FISPACT-II or similar inventory codes, but it is difficult and rare to obtain direct experimental validation of these calculations from neutron irradiation of tungsten (experimental validation of inventory calculations is most commonly done using experimental measurements of quantities derived from the nuclide inventory – e.g. from decay heat measurements [28]). This work will uniquely employ X-ray and gamma-ray spectroscopy in order to verify FISPACT-II modelling results.

1.3. The effect of irradiation on the BDT in tungsten

Table 1 summarises the available data for the effects of neutron irradiation on fracture properties in tungsten. All the experiments were carried out on well-annealed pure tungsten so the BDTT before irradiation would be expected to be around 400–500 K as established by Giannattasio and Roberts [16]. The tests were all carried out using tensile testing and the inferred BDTT was taken as the lowest ductile (>5% strain before fracture) test temperature. The results show a decrease in ductility and a significant increase in the BDTT with irradiation [29]. However, no clear dose dependence could be established and the impact of neutron irradiation would be expected to vary with irradiation temperature [30].

These data are rather limited in several ways: firstly, all the irradiation temperatures are significantly below those expected in a fusion environment (>1073 K) [33]; secondly, only neutron fluences were considered and damage estimates in dpa are not possible from the data provided; finally, there is a lack of analysis of the BDT, only very approximate BDTT values could be inferred from the data and there is no analysis of the strain rate dependence. Only Steichen [29] carried out mechanical testing at multiple strain rates

Table 1
Inferred increases in BDTT from previous mechanical tests on neutron-irradiated tungsten.

Reference	Neutron Fluence(s)/m^{-2}	Irradiation Temperature/K	Strain rate/s^{-1}	BDTT before irradiation/K	Inferred BDTT/K
Steichen [29]	5×10^{25} (E > 0.1 MeV)	644	3×10^{-4}	400	700
	9×10^{25} (E > 0.1 MeV)	655			700
Rau et al. [31]	5.9×10^{22} (E > 1 MeV)	343	Not available	<673	<673
	3.8×10^{23} (E > 1 MeV)				673
	1.2×10^{25} (E > 1 MeV)				>673
Gorynin et al. [32]	1×10^{25} (No threshold energy given)	573	Not available	<573	>773
	2×10^{26}	973			>773

and the BDTT cannot be identified at most strain rates from the data in this work.

It is generally assumed that tungsten will become more brittle after even low dose irradiation [34]. While a small degree of embrittlement might not affect the operational lifetime of ITER, DEMO and future power reactors will have to operate reliably for much longer periods (decades) and to much higher radiation doses [35]. For example, the "second" tritium breeder blanket of DEMO is required to last for almost 15 years and withstand up to 50 dpa [36] (in steel; the value for tungsten would still be of the order of 30 dpa). A greater understanding of the impact of neutron irradiation on the BDT is required if tungsten is to be used as a plasma-facing material.

The experiments described in this paper are the first to characterise fully the increase in BDT following neutron irradiation and its underlying mechanisms.

1.4. Modelling the irradiation induced increase in BDTT

As discussed above, irradiation damage will introduce voids, precipitates and dislocations loops in tungsten. These will act as obstacles to dislocation motion. The model by Swinburne and Dudarev predicts that if this obstacle spacing decreases sufficiently then a doubling of the BDTT would be expected following irradiation (from around 400 K–800 K), along with a doubling of the activation energy from a single to double kink formation.

An alternative explanation for the increase in BDTT in Fe-2.5Cr (also BCC) was proposed by Yi and Robertson [37] based upon dislocation dynamics modelling. Under this model, cross-slip of dislocations is required to unpin dislocations from irradiation-induced obstacles. This significantly reduces the effective dislocation mobility. Since dislocation mobility is temperature dependent this decrease in dislocation mobility can be described as a defect induced apparent temperature shift (ΔDIAT). ΔDIAT was shown to match the change in BDTT for several experiments on Fe–Cr.

Similar to the Swinburne and Dudarev model the BDTT would be expected to increase with irradiation induced defect density. However, the activation energy for the BDT in tungsten would not be expected to change following irradiation, as thermally activated slip of 1/2<111> screw dislocations (controlled by double kink formation) remains the controlling mechanism.

The work in this paper aims to establish the activation energy of the BDT after irradiation and so will provide evidence to distinguish between these models.

2. Experimental

2.1. Sample preparation

Single crystals of commercially pure W were sourced from Metal Crystals and Oxides Limited, Cambridge UK. Frost these, samples ($1 \times 1 \times 12$ mm bars) were prepared for four-point bend tests, as described in previous work [16], with sharp pre-cracks of 60 μm depth and a {100} <001> crack system. The cracks produced by this preparation technique were characterised by Murphy et al. [38]. The samples were irradiated in the High Flux Reactor at Petten under Extremat II [39] (as described by Klimenkov et al. [40]). The irradiation took place at 900 °C and lasted for 8 cycles (208 full power days) in positions C7 and C3, in Extremat II drums 3 and 4. The neutron flux was $6.8 \times 10^{18}\ m^{-2}\ s^{-1}$ ($3.6 \times 10^{18}\ m^{-2}\ s^{-1}$, E > 0.1 MeV) for the first location (148 full power days) and $6.6 \times 10^{18}\ m^{-2}\ s^{-1}$ ($3.4 \times 10^{18}\ m^{-2}\ s^{-1}$, E > 0.1 MeV) for the second location (60 full power days), giving a total fluence of $1.21 \times 10^{26}\ m^{-2}$ ($6.5 \times 10^{25}\ m^{-2}$, E > 0.1 MeV).

2.2. Damage and transmutation

Modelling of the irradiation was carried out using the FISPACT-II inventory code [41,42], which simulated the change in composition (transmutation) and predicted the damage (dpa) levels within the sample during the 208 days of exposure [40,43]. This was carried out using a calculated spectrum, provided by NRG, Petten [44], which considered nearby thermal neutron absorbing experiments. The calculated transmutation level was compared to that measured using energy dispersive X-ray spectroscopy (EDS) using a Mira3 XMH scanning electron microscope with an Oxford Instruments X-Max 80 EDS detector at the Materials Research Facility at CCFE. The EDS spectra were taken from a neutron irradiated sample and a standard W - 5 wt% Re sample. Fig. 1a shows the recorded raw EDS spectrum. The rhenium and tungsten Lα peak sizes were compared to calculate the level of rhenium present in the neutron irradiated samples. Fig. 1b shows the fitted Gaussians to the tungsten and rhenium peaks after subtraction of the X-ray background from the raw data.

Damage calculations (obtained from FISPACT-II using a threshold displacement energy $E_d = 55$ eV [45]) indicated that the average across the samples was 1.67 dpa, at a dose rate of 9.3×10^{-8} dpa/s. The calculated final composition of the samples was 98.5 wt% W, 1.4 wt% Re and 0.1 wt% Os. The EDS analysis indicated a composition of 1.2 ± 0.1 wt% Re and 0.1 wt% Os, in good agreement with the FISPACT-II results. No segregation of Re or Os could be detected using SEM techniques; however, previously published analysis of identically irradiated W samples using EDS in the TEM has shown the presence of Re precipitates following the irradiation [40]. Note that the FISPACT-II calculations do not currently propagate the inherent nuclear data (TENDL-2017 [46]) uncertainties to transmutation rates, although the typical % errors on the reaction-rates of the key neutron capture and multiplication reactions (see Ref. [43]) are 5–10%.

An additional comparison between the inventory simulations and the experiment was obtained via two gamma spectroscopy measurements of the samples carried out in the ADRIANA laboratory at CCFE using the Canberra Broad Energy Germanium (BEGe) and Small Anode Germanium (SAGe) well-type high purity germanium detectors [47]. Canberra's Genie 2000 software [48], was used to perform photopeak analysis on two gamma lines; one

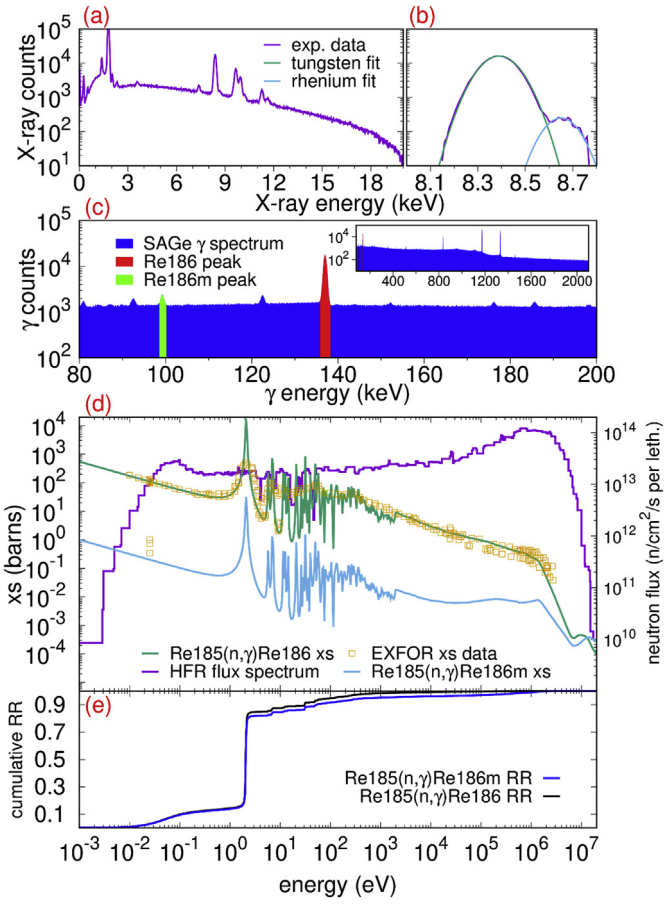

Fig. 1. Transmutation and γ-spectroscopy analysis of the samples. a) raw EDS X-ray spectrum. b) zoomed portion of X-ray spectrum showing Gaussian fit to W-peak at ~8.4 keV and Re peak at 8.65 keV with the comparative areas under each curve indicating the amount of Re in the sample. Note that in (b) the data first had the background counts removed via analysis of the background in the range 8–9 keV for the data in (a). (c) γ-spectroscopy measurements of irradiated samples showing the full spectrum 9inset) and the region below 200 keV with the peaks associated with Re186 activity highlighted. (d) Nuclear cross section (xs) data for neutron capture on Re185 for production of Re186 and its metastable state Re186 m. The data is compared to the available experimental measurements from the EXFOR international database and the simulated HFR flux spectrum experienced by the samples is shown for reference using the right-hand y-axis scale. "per leth." or per lethargy refers to the standard practice of dividing the flux by the logarithm of the energy bin width to remove bias caused when bins have large variation. (e) shows the cumulative reaction rate (RR) of the two neutron capture reactions under the HFR spectrum. See main text for more details.

from ^{186}Re at 137 keV and another from ^{186m}Re at 99 keV. Fig. 1c shows the gamma spectrum measured using the SAGe detector approximately 9 years after the end of the irradiation at Petten. The sample geometry was explicitly modelled for each measurement, and validated MCNP [49] models of the detectors were used to calculate the photopeak efficiencies for each gamma line studied. A 15 cm mounted detection geometry was used with an acquisition time of 474 h on the BEGe detector, and an in-well geometry was used on the SAGe detector, with an acquisition time of 235 h. Specific activities for identified nuclides were then calculated and compared to results from FISPACT II modelling.

The activity measured for the primary detected isotope, ^{186}Re, via the 137 keV peak, was 187 ± 2 Bq g^{-1} (the average of the two detector measurements, with uncertainties based on counting statistics). Measurement of the 99 keV peak for ^{186m}Re was only possible in the low-background, high-geometric efficiency conditions of the SAGe detector; the half-life of ^{186m}Re is 2×10^5 years compared to only 3.7 days for ^{186}Re, and so high detection efficiency and low signal-to-noise ratio are required to produce a meaningful result. The direct ^{186m}Re activity was found to be 200 ± 9 Bq g^{-1}.

The decay-corrected (to account for the ~9 years of cooling) activity calculated by FISPACT-II for both ^{186}Re and ^{186m}Re was 95 Bq g^{-1}, with a nuclear data uncertainty of around 7% (this does not include uncertainties associated with the MCNP modelling or the experiment). Note that after such a long period of cooling the two nuclides are in secular equilibrium since all the original (created under irradiation) ^{186}Re has long since decayed away and only the residual activity feeding from ^{186m}Re remains – hence they have identical activity, as predicted in FISPACT-II simulations.

Fig. 1d shows the nuclear reaction cross section (xs) data associated with the neutron capture cross sections to produce 186 isotopes from ^{185}Re (one of the main stable isotopes produced via transmutation of W). The figure shows that the available experimental data (from EXFOR) is well captured by the reaction associated with the production of ^{186}Re. However, this is not important in this case because only the ^{186m}Re produced during irradiation remains. Clearly, the cross section associated with producing this metastable radioisotope (the blue curve in Fig. 1d) is more uncertain – there is very little experimental data measuring this minor channel, which is understandable given the difficult-to-measure long half-life of this nuclide and the fact that more than 99% of the neutron capture (n,γ) on ^{185}Re is associated with ^{186}Re at sub-keV neutron energies. As the cumulative reaction rate (RR) plot in Fig. 1e shows, the majority of the 186 production is governed by the giant resonance in the cross section at around 2 eV (around 70% of the total RR comes from neutron at this narrow energy). Thus, the results are extremely sensitive to the precise attribution of the cross section in this resonance to the two 186 radioisotopes, but nonetheless the agreements (within a factor of 2) is reasonable given the calculation uncertainties.

2.3. Four-point bend tests

The BDT was characterised using four-point bend tests carried out using a molybdenum rig within a vacuum furnace in the Fusion Materials Laboratory at Karlsruhe Institute of Technology (KIT). The temperature was monitored throughout the tests using thermocouples placed close to the samples. Surface tensile stresses σ were calculated using equation (1):

$$\sigma = 3\,P\,\frac{(L-a)}{2\,w\,t^2}, \tag{1}$$

where P is the applied load, L and a are the outer and inner load spans (10 mm and 5 mm respectively), and w and t are the width and thickness of the beam (both 1 mm). The geometry of the samples is shown in Fig. 2.

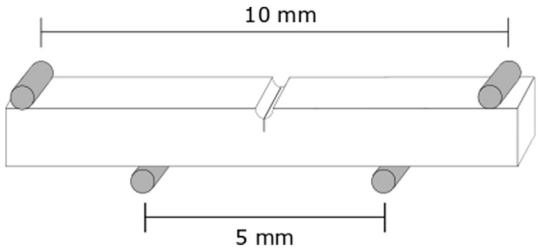

Fig. 2. Geometry of four-point bend tests of 1×1 mm cross-section samples. The samples were loaded such that the notch and pre-cracks were on the tensile face of the specimen.

Surface strain rates were calculated from loading rates in the elastic portion of the loading curve, assuming an elastic modulus of 400 GPa. The tests were carried out under cross-head displacement control at four constant displacement rates, shown in Table 2.

Samples that showed >10% strain before fracture were classified as ductile. This was used instead of a fracture toughness criterion as the limited number of samples available meant that accurate fracture toughness values could not be determined. The fracture surfaces from the four-point bend tests were characterised using SEM at KIT. This allowed confirmation of a sample as either brittle to ductile, giving further confidence in the transition temperature for each strain rate, and allowed comparison of the fracture surfaces from irradiated and unirradiated samples.

The results from four-point bend tests at each strain rate are shown in Fig. 3. At each strain rate, with increasing temperature, a distinct transition from brittle to ductile behaviour was observed. The brittle-ductile transition temperatures (BDTT), taken to be the lowest ductile temperature for each strain rate, are shown in Table 2; BDTT increased with increasing strain rate. The largest uncertainty in the measurements was the temperature range between testing temperatures and so the uncertainty in the BDTT has been taken as the gap between the highest brittle and lowest ductile test temperatures. Fig. 4 compares the BDTT values from these experiments on irradiated tungsten single crystals with those found for unirradiated W single crystal tested using the same method [16]. Where data are available at a comparable strain rate ($\approx 7 \times 10^{-6}$ s^{-1}), neutron irradiation to 1.67 dpa has caused the BDTT to increase by ≈ 500 K.

For unirradiated tungsten, the transition temperature (T_{BDT}) – strain rate ($\dot{\varepsilon}$) relationship was found to follow an Arrhenius relation: equation (2), where A is a constant and k is the Boltzmann constant; the associated activation energy, E_{BDT}, was found to be 1.0 ± 0.05 eV [16,50].

$$\dot{\varepsilon} = A \exp\left(-\frac{E_{BDT}}{kT_{BDT}}\right) \tag{2}$$

The variation of BDTT with strain rate for irradiated tungsten was also found to follow this relation (Fig. 5), with an activation energy of 1.05 ± 0.3 eV, similar to the value for unirradiated tungsten.

Figs. 6 and 7 show SEM micrographs of fracture surfaces are shown for unirradiated [16] and irradiated samples. In both specimen types, at temperatures far below the BDT, fracture is by cleavage on the {001} plane, with little visible deformation, whereas at temperatures close to the BDT rough fracture surfaces with characteristic river lines are observed. Above the BDT, fracture surfaces show significant macroscale deformation; here fracture occurred at strains greater than 10%. The notch and pre-crack are labelled in Fig. 6b and were measured as having depths of 25 μm and 35 μm respectively, agreeing with the values measured during the testing of unirradiated material.

2.4. Nanoindentation: strain-rate jumps

Nanoindentation of both unirradiated and neutron irradiated tungsten was carried out with a Berkovich tip using a Nanoindenter XP (MTS Systems Corporation, Oak Ridge, TN) within the Materials Research Facility at Culham Centre for Fusion Energy. The continuous stiffness measurement technique was used with an oscillation of 2 nm at 45 Hz. Indents were made to a depth of 2000 nm at a target strain rate of 0.05 s^{-1}. Hardness values (averaged over the indentation depth range 800–1800 nm) were 5.0 ± 0.1 GPa for unirradiated tungsten and 7.2 ± 0.1 GPa for irradiated tungsten.

The indentation strain rate sensitivity was measured using the method described by Maier et al. [51]. Four different strain rates were used between 0.01 and 0.1 s^{-1} at indentation depths between 1200 and 2400 nm. A typical hardness response curve is shown in Fig. 8.

Fig. 9 shows hardness results from strain-rate jump tests. These results were analysed using equations (3) and (4) [51], where m = strain-rate sensitivity, H = Hardness, V = activation volume for plastic deformation, σ_f = flow stress and b = magnitude of the Burgers vector. The results from this analysis are shown in Table 3. The activation volume for unirradiated tungsten of 5.6 b^3 agrees well with results from other nanoindentation experiments [52]. The activation volume does not appear to have changed significantly following irradiation.

$$m_{indentation} = \frac{d\,(\ln H)}{d\,\ln(\dot{\varepsilon}\,)} \tag{3}$$

$$m = \frac{\sqrt{3}kT}{V.\sigma_f} \approx \frac{3\sqrt{3}kT}{V.H} \tag{4}$$

3. Discussion

3.1. Transmutation

There is good agreement between the measured rhenium content from EDS, and the level predicted from FISPACT-II inventory modelling. This provides evidence that, with an accurate spectrum, computational modelling can be reliably used to predict transmutation. However, it is essential that an accurate spectrum is used. The initial modelling for this work used an average spectrum for the reactor, resulting in a large error in estimation of transmutation [43]. Only once a location specific spectrum was used, was good agreement between experiment and modelling achieved.

There is a factor of two difference between the simulation-predicted activity of ^{186}Re/^{186m}Re and that measured by gamma-ray spectroscopy. While this at first appears concerning in light of the excellent agreement with the simulated and measured total Re production, there are a number of possible explanations. Firstly, the concentrations of these 186 radioisotopes in comparison to the main Re transmutation products are very low; for example, around

Table 2
Displacement rates, calculated surface strain rates, stress intensity factor rates and brittle-ductile transition temperatures for four-point bend tests on neutron-irradiated tungsten.

Displacement Rate (mm min^{-1})	Surface Strain Rate (s^{-1})	Stress intensity factor rate, $\dot{K}_I$ /MPa $m^{1/2}$ s^{-1}	BDTT (K)
0.0005	3.5×10^{-7}	0.002	723 ± 25
0.001	7×10^{-7}	0.004	773 ± 25
0.01	7×10^{-6}	0.04	898 ± 25
0.035	2.5×10^{-5}	0.15	973 ± 50

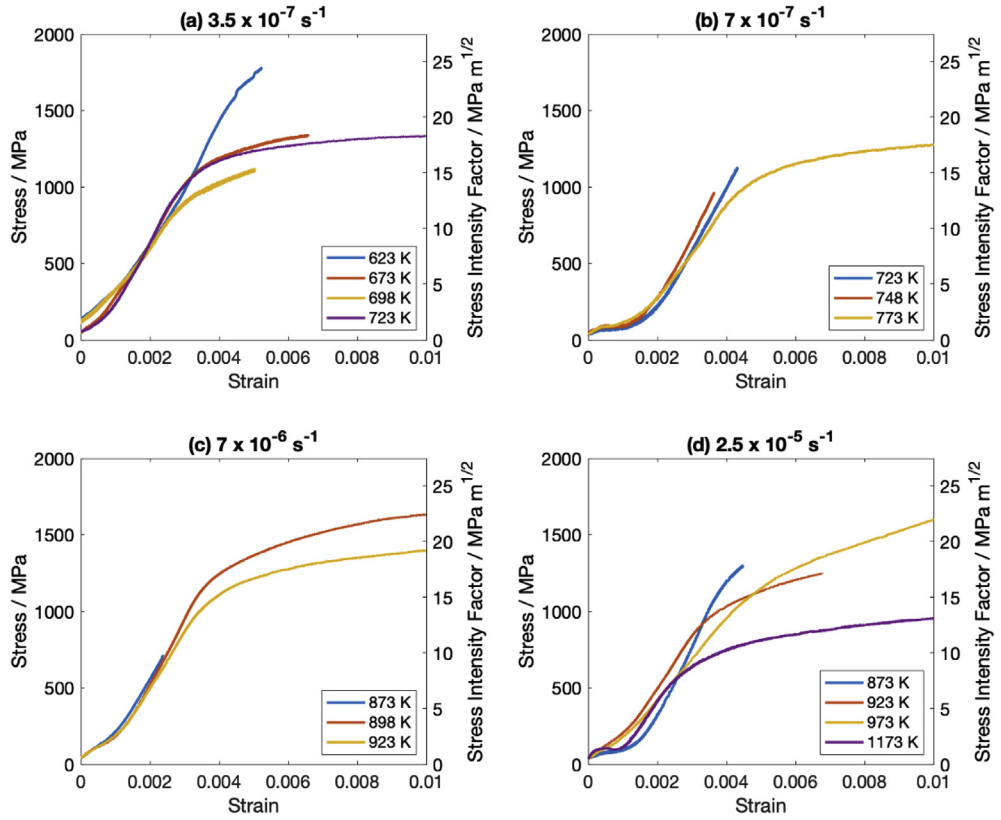

Fig. 3. Four-point bending stress-strain curves for neutron-irradiated single crystal W at a range of temperatures and strain rates. The transition from brittle to ductile behaviour with increasing temperature can be clearly observed at each strain rate.

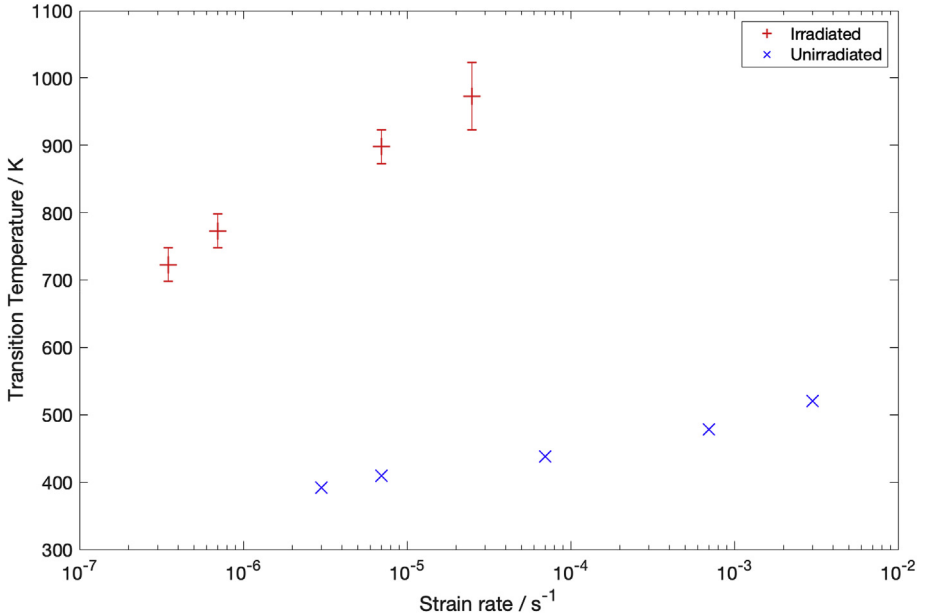

Fig. 4. Comparison of BDTT at a range of strain rates for unirradiated W [7] and neutron irradiated W. Error bars were calculated as the temperature gap between highest brittle test temperature and lowest ductile test temperature.

10^5 times more atoms of ^{187}Re are predicted compared to the slowly decaying ^{186m}Re. Thus, a discrepancy between the model and the gamma spectroscopy result does not necessarily correlate to a significant error in overall transmutation. Secondly, and perhaps more importantly, there is large uncertainty in the nuclear reaction data to produce ^{186m}Re, which is the nuclide being measured (regardless of production rate for the short-lived ^{186}Re). As Fig. 1d and e showed, there is considerable reason to doubt the amount of ^{186m}Re predicted by the simulations and thus a factor of two is not unreasonable.

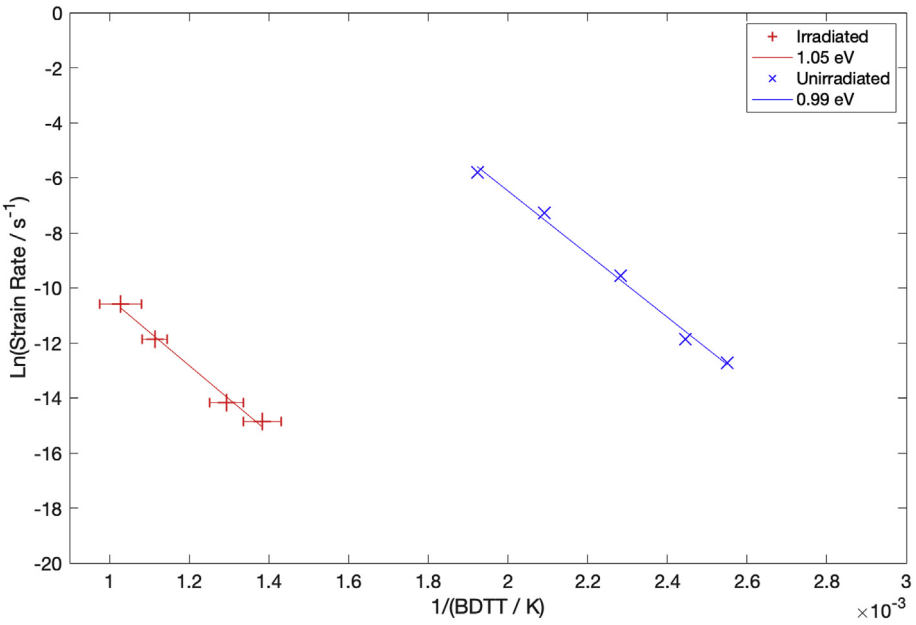

Fig. 5. Arrhenius plot comparing activation energy of BDT in unirradiated W and neutron irradiated W.

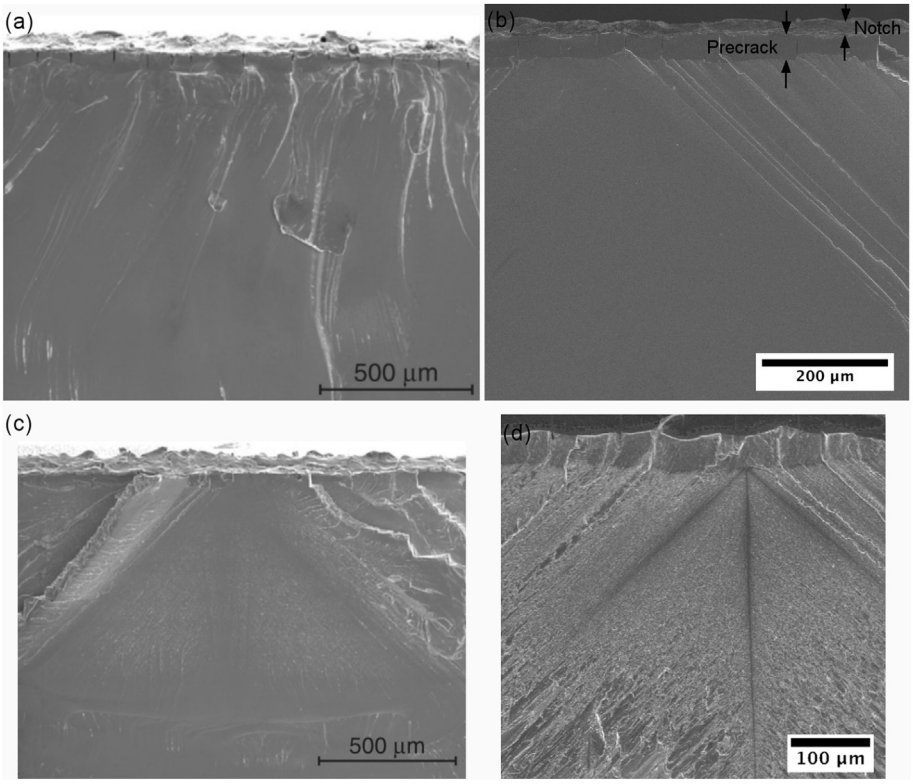

Fig. 6. SEM fractography showing (a) Low ductility observed in unirradiated sample fracture at 77 K with a strain rate of 7 x 10^{-4} s^{-1} [16], (b) Low ductility observed in neutron irradiated sample fracture at 473 K with a strain rate of 7 x 10^{-7} s^{-1}, (c) River lines observed in sample fractured at 478 K with a strain rate of 7 x 10^{-4} s^{-1} (close to BDT) [16], and (d) River lines observed in sample fractured at 723 K with a strain rate of 3.5 x 10^{-7} s^{-1} (close to BDT).

3.2. Irradiation hardening

The results from nanoindentation in this experiment are compared to the previous results from neutron irradiation of single crystal tungsten at similar temperatures in Table 4. Similar irradiation hardening was observed in this experiment as in previous experiments. The irradiation hardening measured in this work is slightly lower than that measured following irradiation to 0.7 dpa in HFIR. This is most likely caused by differences in irradiation spectrum, which have previously been shown to have a strong impact on the hardening observed in tungsten [53]. This makes measurements and calculations of transmutation as carried out in

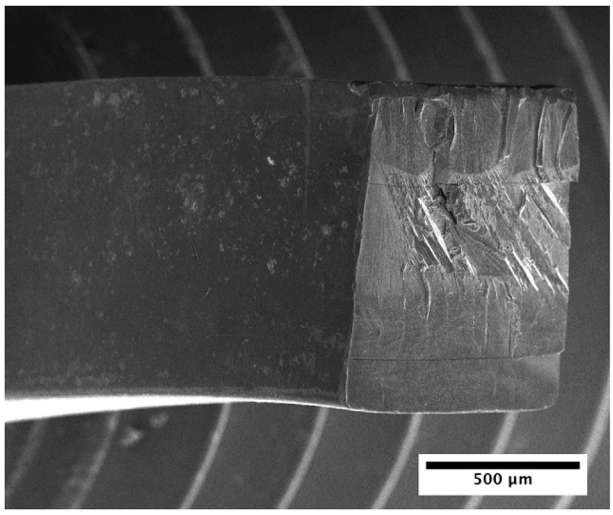

Fig. 7. Low magnification image showing large ductility of neutron irradiated sample before fracture at 823 K with a strain rate of 7×10^{-7} s^{-1}..

this work critical for analysing mechanical properties after neutron irradiation.

The neutron spectrum in HFIR has a strong thermal component and so causes significantly more transmutation (initial rate of 3.4 % Re dpa^{-1}) than that characterised in this work (0.8 %Re dpa^{-1}). For comparison transmutation in DEMO is predicted at a rate of 0.1 %Re dpa^{-1} [54]. As a result a greater density of rhenium precipitates is expected in the material analysed by Fukuda et al. [55] causing greater hardening. It appears that any solution softening from rhenium, as reported for tungsten-rhenium alloys [56], is lost due to precipitate formation under neutron irradiation.

The high temperature of this irradiation may also be affecting the extent of irradiation hardening. Hasegawa et al. [27] showed that temperatures above 700 K enable precipitate and void formation in tungsten under neutron irradiation. This has been backed up by TEM studies of annealing radiation damage in tungsten, which have shown that above 1073 K interstitial dislocation loops grow rapidly and vacancy clusters form voids [57]. Given that the results compared below are all close to or above this temperature, it is likely that the differences in irradiation hardening are caused by the variation in dose and neutron spectrum.

Results from ion irradiation of tungsten from Armstrong et al. [58] are also included for comparison in Table 4. The material investigated in that work was composed of large grains (>50 μm) and was analysed using nanoindentation. As a result, this material is largely equivalent to single crystal. It is clear from the comparison of these results that neutron irradiation has caused significantly greater hardening than ion irradiation. This effect has been highlighted previously [19] and is likely to be associated with the lack of transmutation from ion irradiation.

However, ion irradiation of W – 5Re to 1.2 dpa at 573 K produced only 0.85 GPa of irradiation hardening [58]. That work showed that rhenium clusters were not formed until 33 dpa under ion irradiation, whereas they are commonly observed under neutron irradiation below 1 dpa [19]. This difference in irradiation effects requires further investigation if ion irradiation is to be used to replicate neutron damage in tungsten.

3.3. Brittle to ductile transition

The brittle to ductile transition temperature for single crystal tungsten increased by around 400 K after irradiation to 1.67 dpa. This result correlates well with large increases in hardness observed in this work and elsewhere after neutron irradiation. It also agrees with the limited results available from previous experiments as presented in Table 1. This has significant connotations for future reactor designs as such a large increase in BDTT will limit the operating temperature window for tungsten. Further investigations into the BDTT increase in polycrystalline tungsten are required to understand the full impact of neutron irradiation on the use of tungsten in fusion reactors.

Neutron irradiated BDTT data are only available for a small range of conditions for BCC metals. The largest experimentally observed increase in BDTT for each metal as a proportion of meting point are compared in Fig. 10. These results show that generally unirradiated BCC metals have a BDTT of around 0.1–0.15 T_m that increases to a

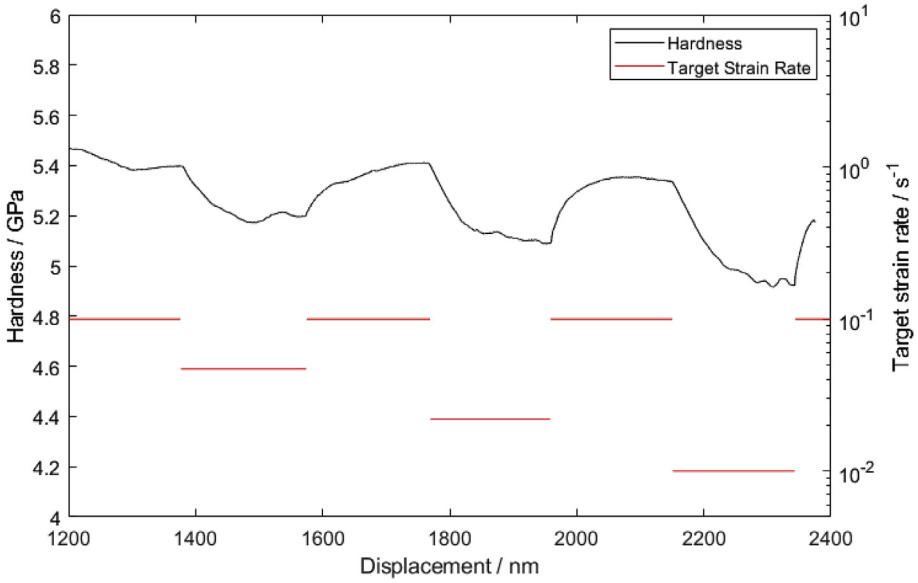

Fig. 8. Hardness versus depth for strain-rate jump tests. The change in hardness corresponding with each decrease and increase in strain rate can be clearly observed. The base strain rate was 0.1 s^{-1} with lower strain rates of 0.047, 0.022 and 0.01 s^{-1}.

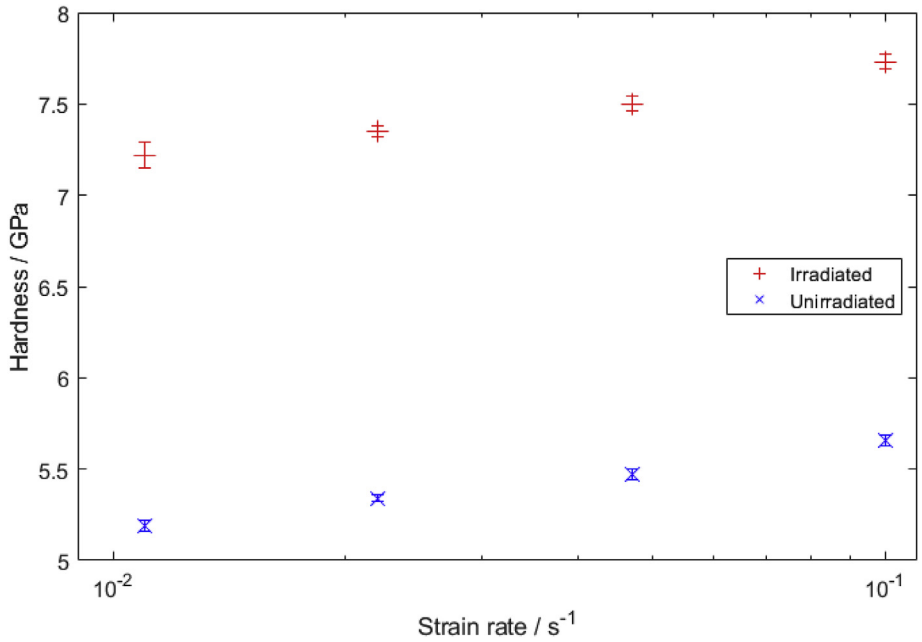

Fig. 9. Results from strain rate jump tests in neutron irradiated and unirradiated tungsten single crystal, showing the increase in measured hardness depending on the applied strain rate.

Table 3
Strain rate sensitivity and activation volume values calculated from strain-rate jump test nanoindentation.

Sample	m	V/m^3	V/b^3
Unirradiated	0.038 ± 0.004	1.1×10^{-28}	5.6 ± 0.7
Neutron Irradiated	0.030 ± 0.007	9.4×10^{-29}	4.6 ± 1.0

maximum of 0.2–0.3 T_m following neutron irradiation. None of these other experiments on neutron irradiated BCC metals characterised the nature of the BDT beyond the increase in temperature so the underlying cause of this increase remains somewhat unclear.

In the experiments report here on initially pure tungsten, neither the activation energy for the BDT, nor the activation volume for dislocation motion during indentation appear to have changed significantly following neutron irradiation. This strongly suggests that the activation mechanism for dislocation mobility has not changed following neutron irradiation. This is despite the presence of voids (diameter $\approx$ 5 nm, number density $\approx 2.5 \times 10^{21}$ m^{-3}) and precipitates (diameter $\approx$ 3–15 nm, number density $\approx 5 \times 10^{21}$ m^{-3}) observed within the microstructure by Klimenkov et al. [40].

It has been shown elsewhere that adding rhenium to tungsten lowers the BDTT, even with rhenium contents as low as 1.9% [62]. This effect has clearly not been seen here following transmutation to 1.4 wt% Re. The work by Klimenkov et al. [40] showed that a high density of rhenium precipitates had formed. However, a volume fraction could not be calculated so it is unknown how much rhenium remains in solution. It is clear that any decrease in BDTT from rhenium in solution has been overwhelmed by other changes in the microstructure during irradiation.

The approximate doubling of the BDTT from $\approx$450 K to $\approx$900 K (depending on strain rate) following neutron irradiation initially appears to agree with the prediction from the model proposed by Swinburne and Dudarev [11]. However, an increase in activation energy from a single kink to double kink energy would be expected and this has not been observed experimentally. Additionally, the activation volume for dislocation motion has remained constant following irradiation, suggesting that the kink mechanism remains the same.

An alternative explanation is that a double kink activation mechanism is acting in the unirradiated and irradiated material. This agrees with the dislocation dynamics modelling carried out by Tarleton and Roberts [17], with the effect of stress acting on the activation volume of the dislocation accounting for the difference between the observed activation energy (1.05 eV) and the theoretical value of 1.75 eV.

In this case, an explanation for the large increase in BDTT without an increase in activation energy is required. The TEM evidence published by Klimenkov et al. [40] shows that a high density of voids and precipitates are present. These defects would significantly reduce the effective dislocation velocity, according to the model suggested by Yi and Robertson [37]. This would result in an increased BDTT, while retaining the kink-pair activation energy. However, further modelling is required to understand whether this mechanism can explain the large increase in BDTT observed in this

Table 4
Irradiation hardening from this experiment compared to other values for single crystal tungsten from Fukuda et al. [53] and Armstrong et al. [58].

Reactor	Fluence/m^{-2} (E > 0.1 MeV)	Dose/dpa	Temperature/K	Irradiation Hardening/GPa	Reference
HFR, Petten	6.5×10^{25}	1.67 (E_d = 55 eV)	1173	2.2	Current study
HFIR, Oak Ridge	5.0×10^{24}	0.15 (E_d = 90 eV)	1073	1.2	[53]
HFIR, Oak Ridge	2.2×10^{25}	0.70 (E_d = 90 eV)	983	3.0	
HFIR, Oak Ridge	9.0×10^{25}	2.88 (E_d = 90 eV)	1043	7.6	
National Ion Beam Centre, Surrey	1.0×10^{18} (W^+ ions)	1.2 (E_d = 68 eV)	573	0.73	[58]

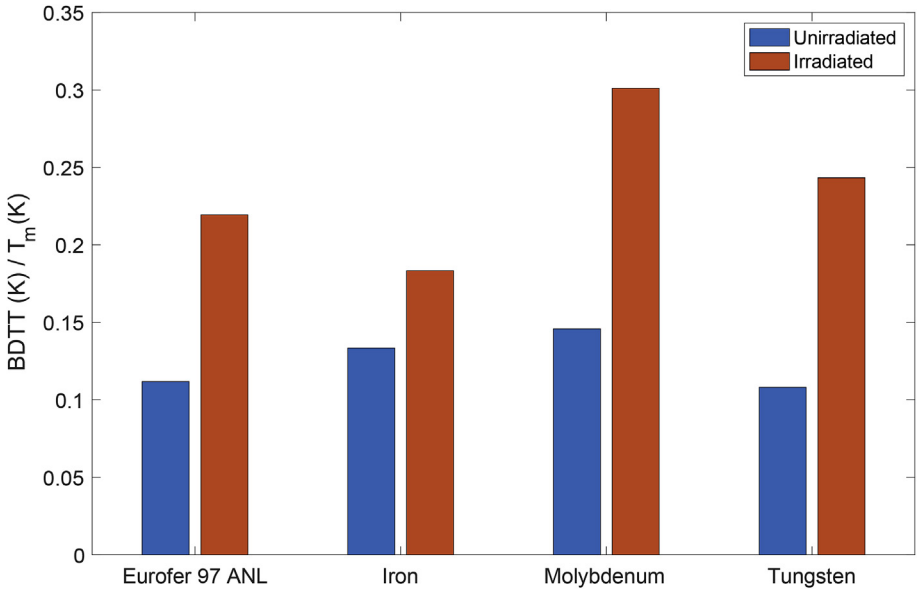

Fig. 10. Increase in BDTT as a proportion of melting point in BCC metals following neutron irradiation. Eurofer 97 ANL was irradiated to 16.3 dpa at 573 K [59], molybdenum to 2.2 dpa at 782 K [60] and iron to 0.4 dpa at 678 K [61].

work.

Understanding the underlying BDT mechanism is critical for predicting how the BDTT will change under irradiated to greater dpa. Data from irradiation of Eurofer-97 shows that the increase in BDTT does not plateau until >10 dpa [59]. This suggests that under fusion conditions, the BDTT of tungsten could increase beyond the values measured in this work, further limiting the operating window for tungsten in a fusion reactor.

4. Conclusions

The level of transmutation in tungsten after neutron irradiation to 1.7 dpa was measured at 1.2 wt% Re, in good agreement with FISPACT-II models, which also matched gamma spectroscopy results to a reasonable degree of accuracy. This is a useful and rare validation of inventory simulations with FISPACT-II and gives confidence in a computational approach that is used widely for analysing transmutation in fission irradiation experiments and for predicting the behaviour of tungsten in future fusion devices.

Four-point bend tests over a range of temperatures and strain rates show that neutron irradiation to 1.7 dpa increases the BDTT relative to that for unirradiated tungsten by approximately 500 K at a strain rate of 7×10^{-6} s^{-1}. This is a critical result for the design of future fusion devices.

Arrhenius analysis of these results shows that the observed activation energy associated with the BDTT has not changed significantly due to irradiation, remaining close to 1.0 eV. This has been identified as the activation energy for motion of 1/2<111> screw dislocations controlling the BDT. Nanoindentation strain-rate jump tests show that the activation volume for dislocation motion has not changed significantly following neutron irradiation.

These results strongly suggest that the controlling mechanism for the BDT in tungsten (the mobility of dislocations near the crack tip) has not changed following neutron irradiation, despite the presence of very fine cavities and precipitates observed by TEM [40]. These results disagree with the latest modelling of the changes in brittle to ductile transition following neutron irradiation [18], which predict a doubling of the activation energy. Instead, a decrease in effective dislocation velocity due to the increased obstacle density is a possible explanation for the large increase in BDTT but further modelling is required.

Data availability

The raw data required to reproduce these findings are available to download from https://doi.org/10.17632/xdftk2np78. The processed data required to reproduce these findings are available to download from https://doi.org/10.17632/8xxw6xtfgr.

Acknowledgements

This work was supported by the UK's Centre for Doctoral Training in Fusion Science, the UK Engineering and Physical Sciences Research Council [EP/L01663X/1] and the European Union FP6 Integrated Project 'Extremat' (contract NMP-CT-2004-500253). Post-irradiation experiments were carried out in the Fusion Materials Laboratory at Karlsruhe Institute of Technology and UKAEA's Materials Research Facility, which has been funded by and is part of the UK's National Nuclear User Facility and Henry Royce Institute for Advanced Materials. CCFE research contributions were funded by the RCUK Energy programme [EP/P012450/1]. DEJA was funded by a RAEng Fellowship.

Appendix A. Supplementary data

Supplementary data to this article can be found online at https://doi.org/10.1016/j.jnucmat.2019.151799.

References

[1] H. Bolt, V. Barabash, W. Krauss, J. Linke, R. Neu, S. Suzuki, N. Yoshida, Materials for the plasma-facing components of fusion reactors, J. Nucl. Mater. 329–333 (2004) 66–73, https://doi.org/10.1016/j.jnucmat.2004.04.005.

[2] P. Norajitra, L.V. Boccaccini, A. Gervash, R. Giniyatulin, N. Holstein, T. Ihli, G. Janeschitz, W. Krauss, R. Kruessmann, V. Kuznetsov, A. Makhankov, I. Mazul, A. Moeslang, I. Ovchinnikov, M. Rieth, B. Zeep, Development of a helium-cooled divertor: material choice and technological studies, J. Nucl. Mater. 367–370 (2007) 1416–1421, https://doi.org/10.1016/j.jnucmat.2007.04.027.

[3] J. Reiser, S. Wurster, J. Hoffmann, S. Bonk, C. Bonnekoh, D. Kiener, R. Pippan, A. Hoffmann, M. Rieth, Ductilisation of tungsten (W) through cold-rolling: R-

curve behaviour, Int. J. Refract. Metals Hard Mater. 58 (2016) 22–33, https://doi.org/10.1016/J.IJRMHM.2016.03.006.
[4] J. Reiser, L. Garrison, H. Greuner, J. Hoffmann, T. Weingärtner, U. Jäntsch, M. Klimenkov, P. Franke, S. Bonk, C. Bonnekoh, S. Sickinger, S. Baumgärtner, D. Bolich, M. Hoffmann, R. Ziegler, J. Konrad, J. Hohe, A. Hoffmann, T. Mrotzek, M. Seiss, M. Rieth, A. Möslang, Ductilisation of tungsten (W): tungsten laminated composites, Int. J. Refract. Metals Hard Mater. 69 (2017) 66–109, https://doi.org/10.1016/J.IJRMHM.2017.07.013.
[5] M. Rieth, S.L. Dudarev, S.M. Gonzalez de Vicente, J. Aktaa, T. Ahlgren, S. Antusch, D.E.J. Armstrong, M. Balden, N. Baluc, M.-F. Barthe, W.W. Basuki, M. Battabyal, C.S. Becquart, D. Blagoeva, H. Boldyryeva, J. Brinkmann, M. Celino, L. Ciupinski, J.B. Correia, A. De Backer, C. Domain, E. Gaganidze, C. Garcia-Rosales, J. Gibson, M.R. Gilbert, S. Giusepponi, B. Gludovatz, H. Greuner, K. Heinola, T. Höschen, A. Hoffmann, N. Holstein, F. Koch, W. Krauss, H. Li, S. Lindig, J. Linke, C. Linsmeier, P. Lopez-Ruiz, H. Maier, J. Matejicek, T.P. Mishra, M. Muhammed, A. Munoz, M. Muzyk, K. Nordlund, D. Nguyen-Manh, J. Opschoor, N. Ordas, T. Palacios, G. Pintsuk, R. Pippan, J. Reiser, J. Riesch, S.G. Roberts, L. Romaner, M. Rosiński, M. Sanchez, W. Schulmeyer, H. Traxler, A. Urena, J.G. van der Laan, L. Veleva, S. Wahlberg, M. Walter, T. Weber, T. Weitkamp, S. Wurster, M.A. Yar, J.H. You, A. Zivelonghi, A brief summary of the progress on the EFDA tungsten materials program, J. Nucl. Mater. 442 (2013) S173–S180, https://doi.org/10.1016/j.jnucmat.2013.03.062.
[6] C. Linsmeier, M. Rieth, J. Aktaa, T. Chikada, A. Hoffmann, J. Hoffmann, A. Houben, H. Kurishita, X. Jin, M. Li, A. Litnovsky, S. Matsuo, A. von Müller, V. Nikolic, T. Palacios, R. Pippan, D. Qu, J. Reiser, J. Riesch, T. Shikama, R. Stieglitz, T. Weber, S. Wurster, J.-H. You, Z. Zhou, Development of advanced high heat flux and plasma-facing materials, Nucl. Fusion 57 (2017), 092007, https://doi.org/10.1088/1741-4326/aa6f71.
[7] D. Rupp, S.M. Weygand, Anisotropic fracture behaviour and brittle-to-ductile transition of polycrystalline tungsten, Philos. Mag. 90 (2010) 4055–4069, https://doi.org/10.1080/14786435.2010.504198.
[8] B. Gludovatz, S. Wurster, A. Hoffmann, R. Pippan, Fracture toughness of polycrystalline tungsten alloys, Int. J. Refract. Metals Hard Mater. 28 (2010) 674–678, https://doi.org/10.1016/j.ijrmhm.2010.04.007.
[9] S. Zinkle, N. Ghoniem, Operating temperature windows for fusion reactor structural materials, Fusion Eng. Des. 51–52 (2000) 55–71, https://doi.org/10.1016/S0920-3796(00)00320-3.
[10] M.R. Gilbert, S.L. Dudarev, S. Zheng, L.W. Packer, J.C. Sublet, An integrated model for materials in a fusion power plant: transmutation, gas production, and helium embrittlement under neutron irradiation, Nucl. Fusion 52 (2012), https://doi.org/10.1088/0029-5515/52/8/083019.
[11] R. Villari, V. Barabash, F. Escourbiac, L. Ferrand, T. Hirai, V. Komarov, M. Loughlin, M. Merola, F. Moro, L. Petrizzi, S. Podda, E. Polunovsky, G. Brolatti, Nuclear analysis of the ITER full-tungsten divertor, Fusion Eng. Des. 88 (2013) 2006–2010, https://doi.org/10.1016/j.fusengdes.2013.02.156.
[12] T.L. Johnston, R.G. Davies, N.S. Stoloff, Slip character and the ductile to brittle transition of single-phase solids, Philos. Mag. 12 (1965) 305–317, https://doi.org/10.1080/14786436508218873.
[13] P. Gumbsch, Controlling factors for the brittle-to-ductile transition in tungsten single crystals, Science 282 (1998) 1293–1295, https://doi.org/10.1126/science.282.5392.1293 (80-.).
[14] P. Gumbsch, Brittle fracture and the brittle-to-ductile transition of tungsten, J. Nucl. Mater. 323 (2003) 304–312, https://doi.org/10.1016/j.jnucmat.2003.08.009.
[15] A.A.N. Németh, J. Reiser, D.E.J. Armstrong, M. Rieth, The nature of the brittle-to-ductile transition of ultra fine grained tungsten (W) foil, Int. J. Refract. Metals Hard Mater. 50 (2015) 9–15, https://doi.org/10.1016/j.ijrmhm.2014.11.005.
[16] A. Giannattasio, S.G. Roberts, Strain-rate dependence of the brittle- to-ductile transition temperature in tungsten, Philos. Mag. 87 (2007) 37–41, https://doi.org/10.1080/14786430701253197.
[17] E. Tarleton, S.G. Roberts, Dislocation dynamic modelling of the brittle–ductile transition in tungsten, Philos. Mag. 89 (2009) 2759–2769. http://www.tandfonline.com/doi/pdf/10.1080/14786430902992619. (Accessed 18 August 2015).
[18] T.D. Swinburne, S.L. Dudarev, Kink-limited Orowan strengthening explains the brittle to ductile transition of irradiated and unirradiated bcc metals, Phys. Rev. Mater. 2 (2018), 073608, https://doi.org/10.1103/PhysRevMaterials.2.073608.
[19] R.G. Abernethy, Predicting the performance of tungsten in a fusion environment: a literature review, Mater. Sci. Technol. 33 (2017) 388–399, https://doi.org/10.1080/02670836.2016.1185260.
[20] M. Rieth, S.L. Dudarev, S.M. Gonzalez de Vicente, J. Aktaa, T. Ahlgren, S. Antusch, D.E.J. Armstrong, M. Balden, N. Baluc, M.-F. Barthe, W.W. Basuki, M. Battabyal, C.S. Becquart, D. Blagoeva, H. Boldyryeva, J. Brinkmann, M. Celino, L. Ciupinski, J.B. Correia, A. De Backer, C. Domain, E. Gaganidze, C. García-Rosales, J. Gibson, M.R. Gilbert, S. Giusepponi, B. Gludovatz, H. Greuner, K. Heinola, T. Höschen, A. Hoffmann, N. Holstein, F. Koch, W. Krauss, H. Li, S. Lindig, J. Linke, C. Linsmeier, P. López-Ruiz, H. Maier, J. Matejicek, T.P. Mishra, M. Muhammed, A. Muñoz, M. Muzyk, K. Nordlund, D. Nguyen-Manh, J. Opschoor, N. Ordás, T. Palacios, G. Pintsuk, R. Pippan, J. Reiser, J. Riesch, S.G. Roberts, L. Romaner, M. Rosiński, M. Sanchez, W. Schulmeyer, H. Traxler, A. Ureña, J.G. van der Laan, L. Veleva, S. Wahlberg, M. Walter, T. Weber, T. Weitkamp, S. Wurster, M.A. Yar, J.H. You, A. Zivelonghi, Recent progress in research on tungsten materials for nuclear fusion applications in Europe, J. Nucl. Mater. 432 (2012) 482–500, https://doi.org/10.1016/j.jnucmat.2012.08.018.
[21] M.R. Gilbert, J.-C. Sublet, Neutron-induced transmutation effects in W and W-alloys in a fusion environment, Nucl. Fusion 51 (2011), 043005, https://doi.org/10.1088/0029-5515/51/4/043005.
[22] T. Troev, N. Nankov, T. Yoshiie, Simulation of displacement cascades in tungsten irradiated by fusion neutrons, Nucl. Instrum. Methods Phys. Res. Sect. B Beam Interact. Mater. Atoms 269 (2011) 566–571, https://doi.org/10.1016/j.nimb.2011.01.010.
[23] R.C. Rau, R.L. Ladd, J. Moteff, Voids in irradiated tungsten and molybdenum, J. Nucl. Mater. 33 (1969) 324–327, https://doi.org/10.1016/0022-3115(69)90029-4.
[24] R.K. Williams, F.W. Wiffen, J. Bentley, J.O. Stiegler, Irradiation induced precipitation in tungsten based, W-Re alloys, Metall. Trans. A. 14A (1983) 655–666, https://doi.org/10.1007/BF02643781.
[25] S.J. Zinkle, L.L. Snead, Designing radiation resistance in materials for fusion energy*, Annu. Rev. Mater. Res. 44 (2014) 241–267, https://doi.org/10.1146/annurev-matsci-070813-113627.
[26] M. Fukuda, T. Tanno, S. Nogami, A. Hasegawa, Effects of Re content and fabrication process on microstructural changes and hardening in neutron irradiated tungsten, Mater. Trans. 53 (2012) 2145–2150, https://doi.org/10.2320/matertrans.MBW201110.
[27] A. Hasegawa, M. Fukuda, K. Yabuuchi, S. Nogami, Neutron irradiation effects on the microstructural development of tungsten and tungsten alloys, J. Nucl. Mater. 471 (2015) 175–183, https://doi.org/10.1016/j.jnucmat.2015.10.047.
[28] M.R. Gilbert, J.-C. Sublet, Experimental decay-heat simulation-benchmark for 14 MeV neutrons & complex inventory analysis with FISPACT-II, Nucl. Fusion (2019), https://doi.org/10.1088/1741-4326/ab278a.
[29] J.M. Steichen, Tensile properties of neutron irradiated TZM and tungsten, J. Nucl. Mater. 60 (1976) 13–19, https://doi.org/10.1016/0022-3115(76)90112-4.
[30] J. Davis, V. Barabash, A. Makhankov, L. Plöchl, K. Slattery, Assessment of tungsten for use in the ITER plasma facing components, J. Nucl. Mater. 258–263 (1998) 308–312, https://doi.org/10.1016/S0022-3115(98)00285-2.
[31] R.C. Rau, J. Moteff, R.L. Ladd, Comparison of microstructure with mechanical properties of irradiated tungsten, J. Nucl. Mater. 24 (1967) 164–173, https://doi.org/10.1016/0022-3115(67)90005-0.
[32] I.V. Gorynin, V.A. Ignatov, V.V. Rybin, S.A. Fabritsiev, V.A. Kazakov, V.P. Chakin, V.A. Tsykanov, V.R. Barabash, Y.G. Prokofyev, Effects of neutron irradiation on properties of refractory metals, J. Nucl. Mater. 191–194 (1992) 421–425, https://doi.org/10.1016/S0022-3115(09)80079-2.
[33] D. Stork, P. Agostini, J.L. Boutard, D. Buckthorpe, E. Diegele, S.L. Dudarev, C. English, G. Federici, M.R. Gilbert, S. Gonzalez, A. Ibarra, C. Linsmeier, A. Li Puma, G. Marbach, P.F. Morris, L.W. Packer, B. Raj, M. Rieth, M.Q. Tran, D.J. Ward, S.J. Zinkle, Developing structural, high-heat flux and plasma facing materials for a near-term DEMO fusion power plant: the EU assessment, J. Nucl. Mater. 455 (2014) 277–291, https://doi.org/10.1016/j.jnucmat.2014.06.014.
[34] V. Barabash, G. Federici, M. Rödig, L.L. Snead, C.H. Wu, Neutron irradiation effects on plasma facing materials, J. Nucl. Mater. 283–287 (2000) 138–146, https://doi.org/10.1016/S0022-3115(00)00203-8.
[35] J. Riesch, M. Aumann, J.W. Coenen, H. Gietl, G. Holzner, T. Höschen, P. Huber, M. Li, C. Linsmeier, R. Neu, Chemically deposited tungsten fibre-reinforced tungsten - the way to a mock-up for divertor applications, Nucl. Mater. Energy. 9 (2016) 75–83, https://doi.org/10.1016/j.nme.2016.03.005.
[36] G. Federici, W. Biel, M.R. Gilbert, R. Kemp, N. Taylor, R. Wenninger, European DEMO design strategy and consequences for materials, Nucl. Fusion 57 (2017), 092002, https://doi.org/10.1088/1741-4326/57/9/092002.
[37] Y. Li, C. Robertson, Irradiation defect dispersions and effective dislocation mobility in strained ferritic grains: a statistical analysis based on 3D dislocation dynamics simulations, J. Nucl. Mater. 504 (2018) 84–93, https://doi.org/10.1016/J.JNUCMAT.2018.03.026.
[38] J.D. Murphy, A.J. Wilkinson, S.G. Roberts, Characterisation of plastic zones around crack-tips in pure single-crystal tungsten using electron backscatter diffraction, IOP Conf. Ser. Mater. Sci. Eng. 3 (2009), https://doi.org/10.1088/1757-899X/3/1/012015.
[39] C. Linsmeier, Extremat, (n.d.). http://www.extremat.org (accessed April 25, 2019).
[40] M. Klimenkov, U. Jantsch, M. Rieth, H.C. Schneider, D.E.J. Armstrong, J. Gibson, S.G. Roberts, Effect of neutron irradiation on the microstructure of tungsten, Nucl. Mater. Energy. 9 (2016) 480–483, https://doi.org/10.1016/j.nme.2016.09.010.
[41] J.-C. Sublet, J.W. Eastwood, J.G. Morgan, M.R. Gilbert, M. Fleming, W. Arter, FISPACT-II: an advanced simulation system for activation, Transmutation Mater. Model. Nucl. Data Sheets 139 (2017), https://doi.org/10.1016/j.nds.2017.01.002.
[42] M. Fleming, T. Stainer, M.R. Gilbert, The FISPACT-II User Manual, 2018.
[43] M.R. Gilbert, J.-C. Sublet, S.L. Dudarev, Spatial heterogeneity of tungsten transmutation in a fusion device, Nucl. Fusion 57 (2017), 044002, https://doi.org/10.1088/1741-4326/aa5e2e.
[44] S. van der Marck, Private Communication, 2015.
[45] D.R. Mason, X. Yi, M.A. Kirk, S.L. Dudarev, Elastic trapping of dislocation loops in cascades in ion-irradiated tungsten foils, J. Phys. Condens. Matter 26 (2014) 375701, https://doi.org/10.1088/0953-8984/26/11/115701.

[46] A.J. Koning, D. Rochman, J.-C. Sublet, N. Dzysiuk, M. Fleming, S. van der Marck, TENDL: complete nuclear data library for innovative nuclear science and Technology, Nucl. Data Sheets 155 (2019) 1–55, https://doi.org/10.1016/J.NDS.2019.01.002.
[47] Miron Technologies (Caberra) Inc, Broad Energy Germanium Detectors (BEGe), 2016.
[48] Miron Technologies (Caberra) Inc, Genie 2000 Gamma Analysis Software, 2016.
[49] MCNP6 User Manual, 2013, Version 1.0.
[50] A. Giannattasio, Z. Yao, E. Tarleton, S.G. Roberts, Brittle-ductile transitions in polycrystalline tungsten, Philos. Mag. 90 (2010) 3947–3959, https://doi.org/10.1080/14786435.2010.502145.
[51] V. Maier, K. Durst, J. Mueller, B. Backes, H.W. Höppel, M. Göken, Nano-indentation strain-rate jump tests for determining the local strain-rate sensitivity in nanocrystalline Ni and ultrafine-grained Al, J. Mater. Res. 26 (2011) 1421–1430, https://doi.org/10.1557/jmr.2011.156.
[52] D. Kiener, R. Fritz, M. Alfreider, A. Leitner, R. Pippan, V. Maier-Kiener, Rate limiting deformation mechanisms of bcc metals in confined volumes, Acta Mater. 166 (2019) 687–701, https://doi.org/10.1016/J.ACTAMAT.2019.01.020.
[53] M. Fukuda, N.A.P. Kiran Kumar, T. Koyanagi, L.M. Garrison, L.L. Snead, Y. Katoh, A. Hasegawa, Neutron energy spectrum influence on irradiation hardening and microstructural development of tungsten, J. Nucl. Mater. 479 (2016) 249–254, https://doi.org/10.1016/j.jnucmat.2016.06.051.
[54] C.-H. Huang, M.R. Gilbert, J. Marian, Simulating irradiation hardening in tungsten under fast neutron irradiation including Re production by transmutation, J. Nucl. Mater. 499 (2018) 204–215, https://doi.org/10.1016/J.JNUCMAT.2017.11.026.
[55] M. Fukuda, K. Yabuuchi, S. Nogami, A. Hasegawa, T. Tanaka, Microstructural development of tungsten and tungsten–rhenium alloys due to neutron irradiation in HFIR, J. Nucl. Mater. 455 (2014) 460–463, https://doi.org/10.1016/j.jnucmat.2014.08.002.
[56] C. Ren, Z.Z. Fang, M. Koopman, B. Butler, J. Paramore, S. Middlemas, Methods for improving ductility of tungsten - a review, Int. J. Refract. Metals Hard Mater. (2018), https://doi.org/10.1016/j.ijrmhm.2018.04.012.
[57] F. Ferroni, X. Yi, K. Arakawa, S.P. Fitzgerald, P.D. Edmondson, S.G. Roberts, High temperature annealing of ion irradiated tungsten, Acta Mater. 90 (2015) 380–393, https://doi.org/10.1016/j.actamat.2015.01.067.
[58] D.E.J. Armstrong, X. Yi, E.A. Marquis, S.G. Roberts, Hardening of self ion implanted tungsten and tungsten 5-wt% rhenium, J. Nucl. Mater. 432 (2013) 428–436, https://doi.org/10.1016/j.jnucmat.2012.07.044.
[59] E. Gaganidze, H.C. Schneider, B. Dafferner, J. Aktaa, High-dose neutron irradiation embrittlement of RAFM steels, J. Nucl. Mater. 355 (2006) 83–88, https://doi.org/10.1016/j.jnucmat.2006.04.014.
[60] B.V. Cockeram, T.S. Byun, K.J. Leonard, J.L. Hollenbeck, L.L. Snead, Post-irradiation fracture toughness of unalloyed molybdenum, ODS molybdenum, and TZM molybdenum following irradiation at 244 C to 507 C, J. Nucl. Mater. 440 (2013) 382–413, https://doi.org/10.1016/j.jnucmat.2013.05.027.
[61] I. Belianov, P. Marmy, The effect of low dose irradiation on the impact fracture energy and tensile properties of pure iron and two ferritic martensitic steels, J. Nucl. Mater. 258–263 (1998) 1259–1263, https://doi.org/10.1016/S0022-3115(98)00193-7.
[62] D. Klopp, William, W.R. Witzke, P.L. Raffo, Mechanical dilute properties of tungsten-rhenium, NASA Tech. Note (1966) 1–38.